Electrical characterization and equivalent circuit analysis of (Bi1.5Zn0.5)(Nb0.5Ti1.5)O7 Pyrochlore, a relaxor ceramic

Rozana A. M. Osman and Anthony R. West

Related Articles

High permittivity 0.9Pb(Mg1/3Nb2/3)O3-0.1PbTiO3 relaxor thin films for high-value, wide-temperature capacitor applications
J. Appl. Phys. 112, 054105 (2012)

Stress dependence of thermally driven pyroelectric charge release during FER-FEO phase transformations in [011] cut relaxor ferroelectric crystals
Appl. Phys. Lett. 100, 262909 (2012)

Structure, piezoelectric, and ferroelectric properties of BaZrO3 substituted Bi(Mg1/2Ti1/2)O3-PbTiO3 perovskite
J. Appl. Phys. 111, 104118 (2012)

Enhanced electrocaloric effect in poly(vinylidene fluoride-trifluoroethylene)-based terpolymer/copolymer blends
Appl. Phys. Lett. 100, 222902 (2012)

Dielectric relaxation and electrical conductivity in ferroelectric ceramic/polymer composites around the glass transition
Appl. Phys. Lett. 100, 212903 (2012)

Additional information on J. Appl. Phys.

Journal Homepage: http://jap.aip.org/

Journal Information: http://jap.aip.org/about/about_the_journal

Top downloads: http://jap.aip.org/features/most_downloaded

Information for Authors: http://jap.aip.org/authors

Electrical characterization and equivalent circuit analysis of (Bi$_{1.5}$Zn$_{0.5}$)(Nb$_{0.5}$Ti$_{1.5}$)O$_7$ Pyrochlore, a relaxor ceramic

Rozana A. M. Osman, and Anthony R. West[a)]
Department of Materials Science and Engineering, University of Sheffield, United Kingdom, S1 3JD

The ac impedance of (Bi$_{1.5}$Zn$_{0.5}$)(Nb$_{0.5}$Ti$_{1.5}$)O$_7$, a relaxor ceramic with the pyrochlore structure, has been measured over the temperature range 10–1073 K and analyzed using a combination of traditional, fixed-frequency sweeps of permittivity and tan δ, impedance analysis using resistance-capacitance (RC) circuit combinations and equivalent circuit modeling with the inclusion of a constant phase element (CPE). Low temperature data accurately fit an equivalent circuit containing a parallel R-C-CPE element in series with a capacitor. From the temperature-dependence of the fitted R,C,CPE parameters, a model for the relaxor behavior is obtained. © *2011 American Institute of Physics*. [doi:10.1063/1.3553883]

I. INTRODUCTION

The electrical properties of relaxor ferroelectrics are intermediate between those of first order ferroelectrics which show sharp permittivity maxima as a function of temperature and dielectric materials that show very little temperature dependence of permittivity. It is of interest scientifically to understand the origin of relaxor behavior in which the permittivity and tan δ values are both frequency-dependent and temperature-dependent. Relaxors have applications as materials for multilayer ceramic capacitors[1–4] since they have a high permittivity which exhibits only a small variation with temperature over a wide temperature range.

Electrical property measurements and analyses on relaxors are usually limited to presentation of data as fixed frequency plots of permittivity and tan δ against temperature. While the origin of relaxor behavior is reasonably well understood in terms of formation of polar nanodomains, there appear to be no reports of data analysis in terms of equivalent circuits and consequently, no strategy for modeling of the impedance response. Equivalent circuit analysis can provide a powerful data analysis methodology since: (a) it demonstrates that impedance data can be accurately fitted to an array of R, C circuit elements and (b) assuming that it is possible to attribute the R, C elements to specific features of the sample, then understanding of the origin of the electrical properties is obtained.

This paper reports an analysis of the electrical properties of a bismuth zinc niobate titanate relaxor and demonstrates that it is, indeed, possible to accurately model the data in terms of equivalent circuits that contain, as an essential component, a constant phase element. From the temperature-dependence of the circuit parameters, insight into the physical significance of the CPE is obtained. Pyrochlore phases in the Bi$_2$O$_3$−ZnO−Nb$_2$O$_5$, Ta$_2$O$_5$ systems are of interest because they show high values of permittivity leading to possible microwave dielectric applications.[1,5,6] Recent studies have

shown relaxor behavior at low temperatures in the complex composition (Bi$_{1.5}$Zn$_{0.5}$)(Ti$_{1.5}$Nb$_{0.5}$)O$_7$ (Refs. 6–9); this composition is chosen for study here.

II. EXPERIMENTAL

Bismuth zinc niobate titanate (BZNT), with composition (Bi$_{1.5}$Zn$_{0.5}$)(Ti$_{1.5}$Nb$_{0.5}$)O$_7$ was prepared by conventional solid state synthesis. Bi$_2$O$_3$ (99.9%), ZnO (99.99%), TiO$_2$ (99.9%) and Nb$_2$O$_5$ (99.9%) from Sigma-Aldrich were used as starting materials. The reagents were dried, weighed, mixed and ground using an agate mortar and pestle in an acetone slurry, dried, prereacted at 650 °C for 6 h and then heated at 900 °C for 42 h with intermittent grinding every 12 h. Single phase (Bi$_{1.5}$Zn$_{0.5}$)(Ti$_{1.5}$Nb$_{0.5}$)O$_7$ was detected by x-ray powder diffraction (XRD) using a Stoë STADI P diffractometer with a linear position sensitive detector operating in transmission mode, with a Ge monochromator, Cu Kα_1 (1.5406 Å) radiation, step size 0.01° and 2θ range 10° to 60°.

For electrical characterization, samples were pelleted using an uniaxial press and sintered at 1100 °C for 12 h. Pellet density was 94.62% of the theoretical value. Pt paste was used as electrode and was smeared on opposite pellet faces, dried, decomposed and hardened by gradually heating at 900 °C for 1 h. Impedance spectroscopy (IS) measurement at low temperatures (10–320 K) used an Agilent E4980A with Intelligent Temperature Controller (ITC 503S) and at high temperatures (373–1073 K), a Hewlett Packard 4192A; both sets of measurements covered the frequency range 10 Hz–1 MHz. IS data were modeled with various equivalent electrical circuits using ZView equivalent circuit fitting software.

III. RESULTS

A. Electrical property data: conventional analysis for relaxor materials

Impedance measurements were made over the temperature range 10 K to 1100 K and are presented first in the traditional way for relaxors as fixed frequency values of permittivity ε' and tan δ against temperature in the range 10 to

---

a)Author to whom correspondence should be addressed. Electronic mail: a.r.west@Sheffield.ac.uk.

330 K in Fig. 1. The permittivity data show maxima whose temperature, T_m, increases with increasing frequency and whose magnitude at the maximum, ε'_{max} decreases with increasing temperature. At higher temperatures, above $\sim$120 K, permittivity data are independent of frequency. In the high temperature region of frequency-independent permittivity, the data fit the Curie-Weiss law with an extrapolated T_0 value of $\sim$−640 K [inset to Fig. 1(a)]. A large depression of T_0 below T_m is a characteristic of relaxor behavior. Tan δ data [Figs. 1(b) and 1(c)] are both frequency- and temperature-dependent. They decrease from values as high as e.g., 0.05 at 1 MHz and 10 K to 0.001 at 10 kHz and 100 K.

The dispersions seen in ε'_{max}, (Fig. 1), are typical of relaxor materials and are generally attributed to the presence of polar nanodomains within the crystal structure. The temperature at which the permittivity dispersion commences on cooling is often called the Burns temperature and may signify the onset of nanodomain formation. Another temperature that is commonly identified is the so-called freezing temperature, T_{vf} at which the nanodomains become essentially frozen and unable to respond to an applied field. This temperature is identified by fitting the frequencies, f_m, and temperatures, T_m, of ε'_{max} data to the Vogel-Fulcher Equation:

$$f_m = f_o \exp[-E_a/k(T_m - T_{vf})] \tag{1}$$

where k is Boltzmann's constant, 8.617×10^{-5} eVK^{-1}. A Vogel-Fulcher fit to the ε'_{max} data is shown in Fig. 2 from which $T_{vf} = 10$ K; the activation energy, $E_a = 0.06$ eV is obtained from an Arrhenius plot using the same data (see Fig. 2 inset).
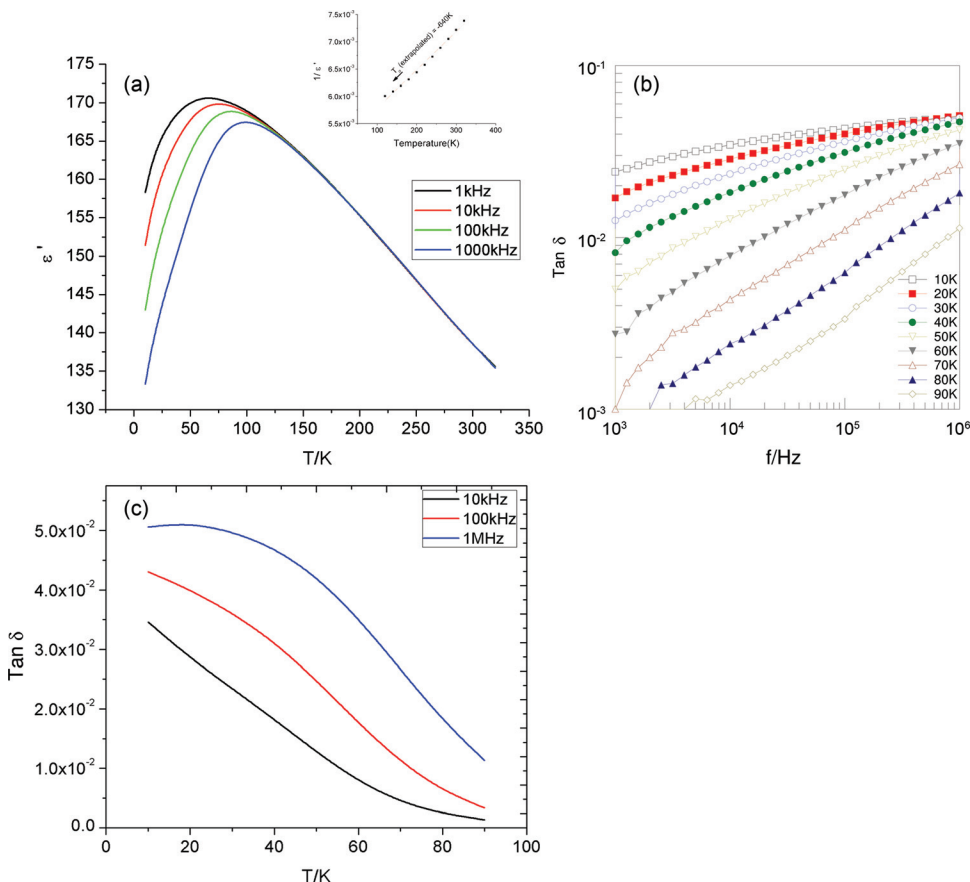
The origin of the nanodomains is attributed to polar regions in the crystal structure whose cooperative alignment is possible over only short distances because of frustration associated with inhomogeneities in either the structure or the composition of the nanodomain regions. In the pyrochlore structure, there are two possible crystallographic sites that could be responsible for the polarity and nanodomain formation. These are the A sites that contain Bi^{3+} and Zn^{2+}, which are two ions of different size and coordination requirements and the octahedral B sites that contain a mixture of Ti^{4+} and Nb^{5+}, which have slightly different sizes. We return to discussion of the possible origins of the relaxor behavior later.

B. Frequency-dependent electrical properties and impedance analysis

The impedance data are, next, analyzed in conventional impedance format as a function of frequency at fixed temperature

1. Low temperature data, 10 – 750 K

Capacitance, C′, data extracted from the impedance measurements are shown as a function of frequency for a selection of temperatures over the range 10 to 1073 K in Fig. 3. At intermediate temperatures, 120–773 K [Figs. 3(c) and 3(d)] the C′ data are independent of frequency and the values decrease with increasing temperature. With decreasing temperature $<\sim$120 K, the C′ data increasingly show a dispersion to lower values with increasing frequency, Fig. 3(b),
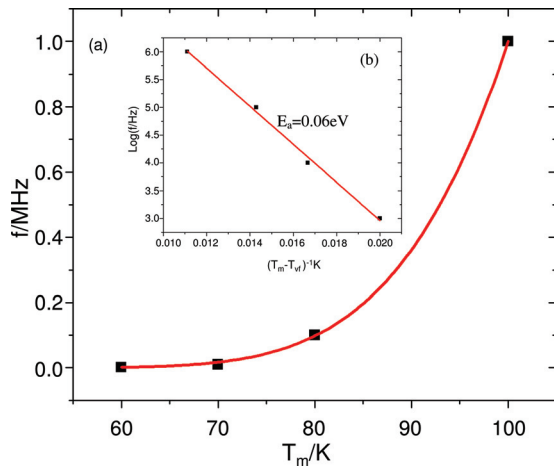

FIG. 1. (Color online) (a) Permittivity vs temperature of $(Bi_{1.5}Zn_{0.5})(Nb_{0.5}Ti_{1.5})O_7$; inset: Curie-Weiss plot; (b) Tan δ vs frequency; (c) Tan δ vs temperature.

FIG. 2. (Color online) Frequencies and temperatures of ε'_{max} with fits to the Vogel-Fulcher equation as (a) f_{max} vs T_{max} and (b) Arrhenius plot of log f_m vs $(T_m - T_{vf})^{-1}$.

and, at the lowest temperatures are frequency-dependent over the entire measurement range, Fig. 3(a).

Admittance or conductivity, Y', data were also extracted from impedance measurements and are shown for a selection of temperatures in the range 10–190 K against frequency on logarithmic scales in Fig. 4(a). The data show frequency-dependent conductivity with an approximately linear, power
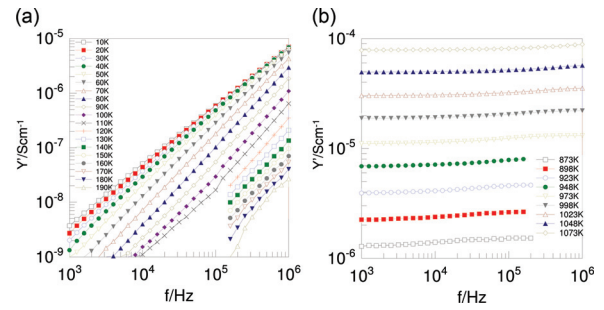

FIG. 4. (Color online) Admittance, Y' vs f for (a) 10–190 K, (b) 873–1073 K.

law dependence with slope n ≈ 1.3 at e.g., 80 K but a curved dependence at lower temperatures. At a given frequency, Y' values decrease with increasing temperature and, for temperatures between 190 and 700 K, not shown, Y' values were too small to extract reliable information from the impedance data. From the nature of the Y' data shown in Fig. 4(a), it was not possible to extract frequency-independent conductivity values for any temperature < 700 K.

2. High temperature data, >∼750 K

At these high temperatures, the Y' data [Fig. 4(b)] were again measurable but showed only small frequency-dependence, from which approximate *dc* conductivity values were estimated. These are plotted in Arrhenius format in Fig. 5. These conductivities represent small leakage conductivities through the sample with a high activation energy, 1.72(1) eV. At the highest temperatures, >∼873 K, an additional low frequency dispersion is seen in the capacitance data [Fig. 3(e)].

3. Circuit analysis

Between ∼120 K and ∼700 K, the impedance data can be modeled by a simple frequency-independent capacitance [see Fig. 3(d) inset]. Below 120 K, additional circuit elements are required to model the frequency-dependent capacitance and the measureable ac conductivity. It is clear that at these lower temperatures, the impedance response departs from that which is usually observed in conducting systems. Thus, the low temperature conductivities [Fig. 4(a)] are ac
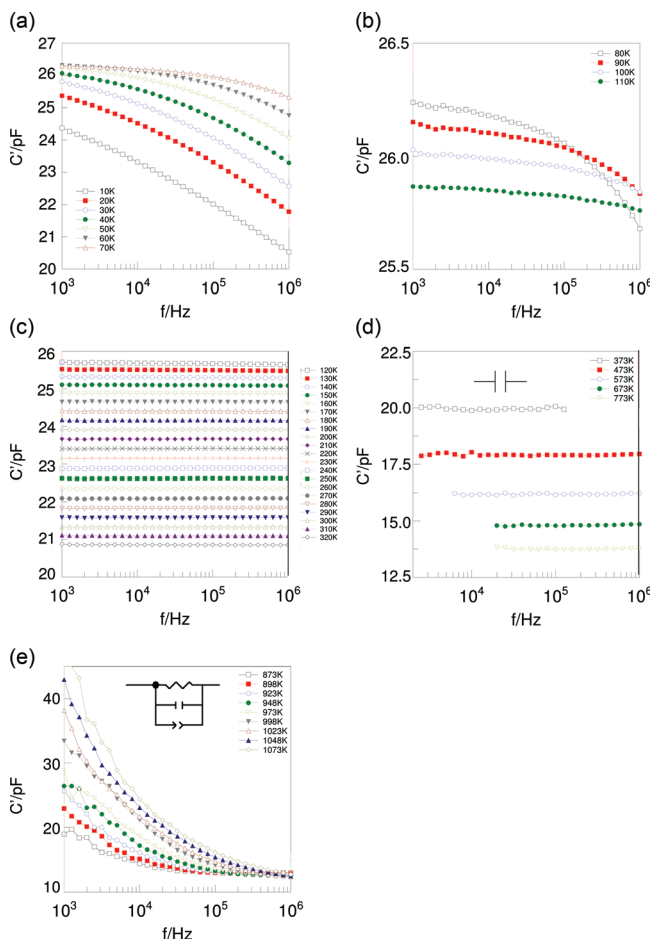

FIG. 3. (Color online) Capacitance, C' vs frequency for (a) 10–70 K, (b) 80–110 K, (c) 120–320 K, (d) 373–773 K, (e) 873–1073 K.
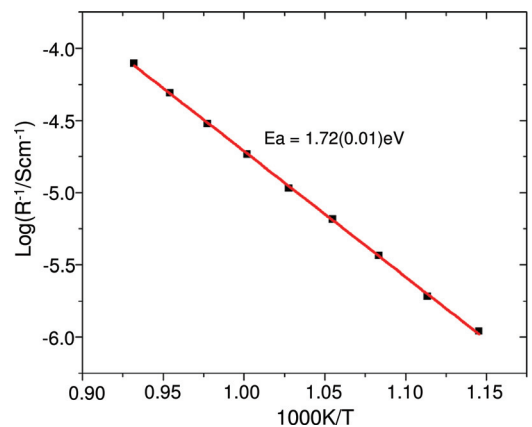

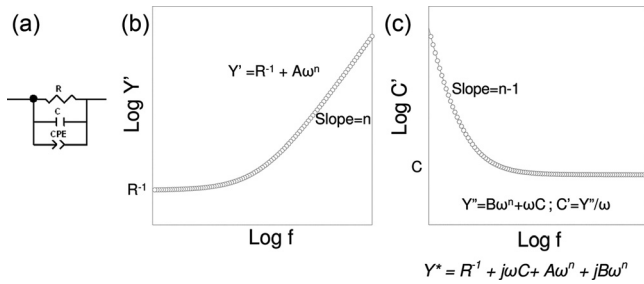FIG. 5. (Color online) Arrhenius plot of R1 for 873–1073 K.

FIG. 6. (a) A parallel R-C-CPE circuit element and its impedance response as (b) log Y′ vs log f and (c) log C′ vs log f.

FIG. 7. Equivalent circuits showing different R, C, CPE combinations.

conductivities with strong frequency dependence and without any evidence of long range, frequency-independent *dc* conduction. Because of the nature of the frequency dependences of C′ and Y′ [Figs. 3(a), 3(b) and 4(a)] modeling the low temperature data in terms of equivalent circuits based on ideal circuit elements with series and/or parallel resistor, R, capacitor, C, combinations is unable to satisfactorily represent the impedance response.

C. Equivalent circuit analysis incorporating constant phase elements

1. Low temperature data

Tests with various R, C circuit combinations showed that it was not possible to model satisfactorily the large dispersions seen in the Y′ and C′ data at low temperatures. The Y′ data show an almost linear, power law dependence on frequency at several temperatures[Fig. 4(a)] which suggests that inclusion of a CPE may be required to fit the data. A CPE takes the form

$$Y^* = A\omega^n + jB\omega^n \qquad (2)$$

where $j = \sqrt{1}$ and

$$B/A = \tan(n\pi/2) \qquad (3)$$

An equivalent circuit that is frequently used to model the electrical properties of ionically conducting materials is shown in Fig. 6(a), and has a parallel combination of a resistor, capacitor and a CPE. This circuit alone cannot model the observed data, however, for several reasons:

First, the slope n of the high frequency power law Y′ data [Fig. 6(b)] is constrained to values between 0 and 1, Eq. (3), whereas the experimental data [Fig. 4(a)] have approximate n values >1.

Second, the Y′ data [Fig. 6(b)] should show frequency-independent values at low frequencies corresponding to *dc* conduction, R^{-1}, through the sample whereas it is clear from the low temperature data [Fig. 4(a)] that there is no evidence for such a *dc* plateau and this resistance, if it exists, is therefore far too large to measure.

Third, the capacitance data [Fig. 6(c)] should show a power law response at low frequencies of slope (n−1) which levels off to a frequency-independent value at high frequencies corresponding to the magnitude of the capacitance C; experimental C′ data clearly do not show this behavior and
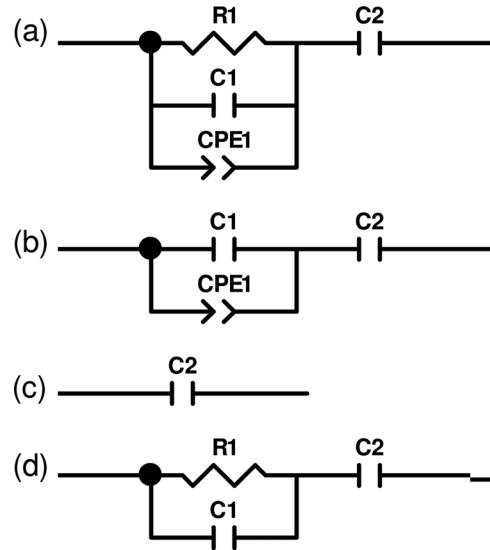
in fact, show the opposite, with a frequency dispersion at high frequencies [Figs. 3(a)–3(b)].

It is clear from the Y′ data shown in Fig. 4(a) and the expected response shown in Fig. 6(b) that the measured conductivities are *ac* conductivities; this means that either resistance R [Fig. 6(a)] is simply too large to measure and can be eliminated from the circuit or a more complex circuit requiring the inclusion of a blocking series capacitance, as shown in circuit Fig. 7(a) or Fig. 7(b), is needed. We find that, depending on temperature, both of these modifications to the equivalent circuit are needed.

For temperatures in the range 10–60 K, the circuit shown in Fig. 7(a) was found to provide an excellent fit to the impedance data, as shown for one example in Fig. 8. All the characteristics of the C′ (a) and Y′ (b) plots are accurately reproduced as are representations of the impedance data in other formalisms (not shown) such as Z″/M″ spectroscopic plots. From the fits at these and other low temperatures, values of the circuit parameters R_1, C_1, C_2, A_1 (and B_1) and n_1 were obtained and are listed in Table I. The magnitude of R_1 decreases with increasing temperature as shown in Fig. 9, and at higher temperatures, e.g., 80 K, R_1 could no longer be modeled as a separate element in circuit Fig. 7(a). The reason for this appears to be that, although R_1 decreases with increasing temperature, the magnitude of the parameter $A\omega^n$,
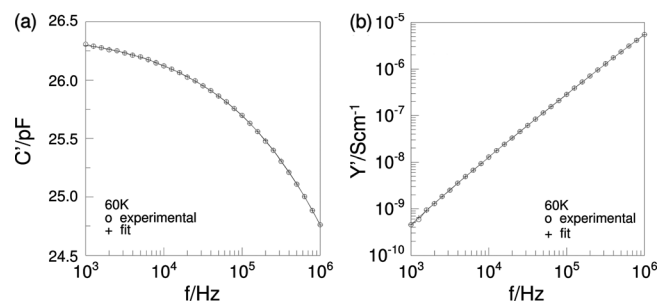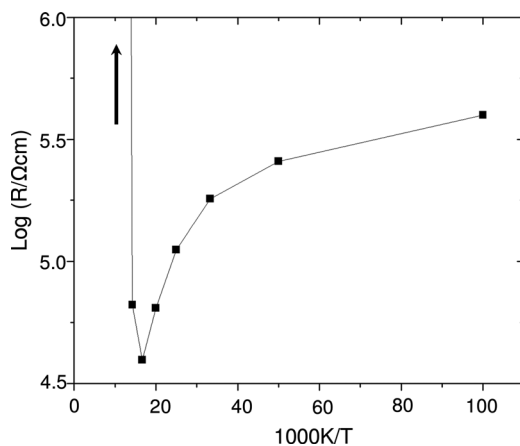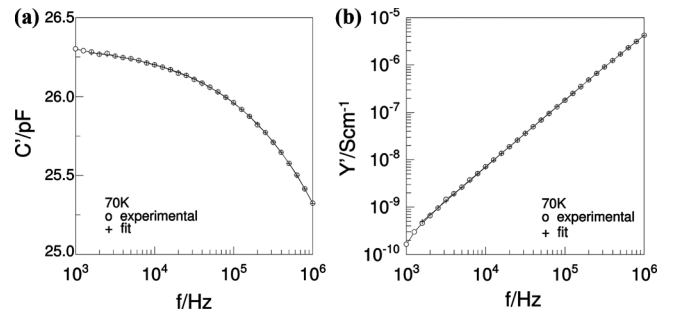

FIG. 8. Fit of the 60 K data to circuit Fig. 7(a) for (a) C′ and (b) Y′.

TABLE I. Fitting data from 10 K to 320 K

Temp (K)	R_1 (Ωcm)	C_1 (Fcm^{-1})	$A(\Omega^{-1}$cm^{-1} rad^{-1})	n	C_2(Fcm^{-1})
10	398040	4.50×10^{-11}	2.88×10^{-9}	0.71134	2.49×10^{-11}
20	257050	4.69×10^{-11}	5.29×10^{-9}	0.69299	2.57×10^{-11}
30	180340	5.03×10^{-11}	9.20×10^{-9}	0.67450	2.60×10^{-11}
40	111420	5.41×10^{-11}	1.70×10^{-8}	0.65459	2.62×10^{-11}
50	64293	5.82×10^{-11}	3.74×10^{-8}	0.62911	2.63×10^{-11}
60	39321	6.88×10^{-11}	1.12×10^{-7}	0.58947	2.63×10^{-11}
70		8.32×10^{-11}	3.77×10^{-7}	0.54717	2.63×10^{-11}
80		1.27×10^{-10}	2.11×10^{-6}	0.49159	2.62×10^{-11}
90		1.55×10^{-10}	7.81×10^{-5}	0.44509	2.61×10^{-11}
100		2.20×10^{-10}	2.36×10^{-5}	0.40851	2.60×10^{-11}
110		3.23×10^{-10}	3.94×10^{-5}	0.40986	2.58×10^{-11}
120					2.57×10^{-11}
130					2.55×10^{-11}
140					2.53×10^{-11}
150					2.51×10^{-11}
160					2.49×10^{-11}
170					2.47×10^{-11}
180					2.43×10^{-11}
190					2.41×10^{-11}
200					2.39×10^{-11}
210					2.36×10^{-11}
220					2.33×10^{-11}
230					2.31×10^{-11}
240					2.28×10^{-11}
250					2.26×10^{-11}
260					2.23×10^{-11}
270					2.20×10^{-11}
280					2.18×10^{-11}
290					2.15×10^{-11}
300					2.13×10^{-11}
310					2.11×10^{-11}
320					2.08×10^{-11}

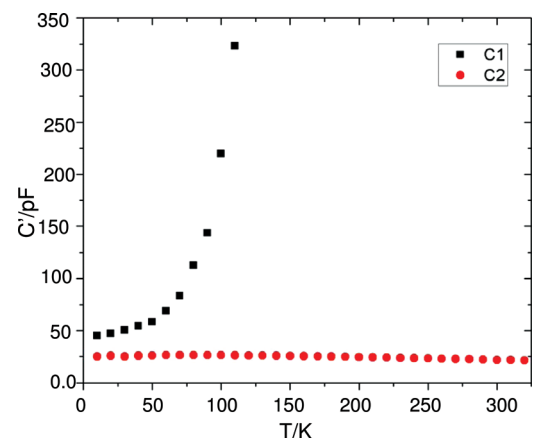FIG. 10. Fit of the 70 K data to circuit Fig. 7(b) for (a) C′ and (b) Y′.

are shown in Fig. 10 with values of the circuit parameters listed in Table I. The curious feature of the data in this temperature range is that the magnitude of capacitance C_1 increased increasingly rapidly as shown in Fig. 11 and effectively was no longer a feasible circuit parameter for temperatures above 110 K. In addition, the magnitude of the CPE A (and B) parameter was such that it could no longer be observed in the frequency range of the measuring instrumentation above 110 K. Thus, for temperatures ≥120 K, the circuit reduced to that of a simple capacitor, circuit Fig. 7(c). The magnitude of capacitance C_2, Table I and Fig. 11, is small and shows very little temperature dependence.

2. High temperature data

The high temperature impedance data >~800 K show a low frequency dispersion in C′, Fig. 3(e). This can be modeled accurately by a parallel R-C-CPE element as shown in Fig. 12. The CPE in this circuit element is very different from the one used in modeling the low temperature data and instead, is associated with the leakage resistance through the sample, which has a frequency-dependent R and C contribution. The C parameter is the same one identified as C_2 in the low temperature data (Fig. 11).

IV. DISCUSSION

The results presented here give new insight into the analysis and understanding of the electrical properties of relaxor materials since it is possible to model the data accurately in terms of equivalent circuits. Permittivity and tan δ

which represents the frequency dependent conductive component of the Y′ data increases more rapidly than the decrease in R_1 and effectively dominates the Y′ data above ~60 K.

For temperatures at and above 70 K, R_1 was therefore eliminated and circuit Fig. 7(b) used to fit the data. Fits of circuit Fig. 7(b) to C′ and Y′ data at one temperature, 70 K,

FIG. 9. Temperature dependence of resistance R_1.

FIG. 11. (Color online) Temperature dependence of fitted capacitances C_1 and C_2.
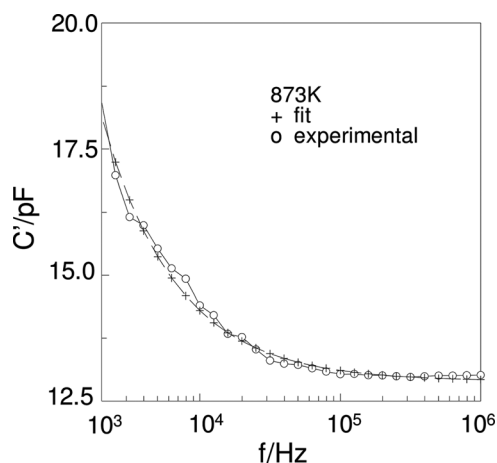
FIG. 12. Fit of high temperature data.

data of relaxors are both frequency- and temperature-dependent and cannot be represented in any obvious way by the usual combinations of R and C circuit elements that are used to model and fit impedance data of both ionic conductors and semiconductors. However, introduction of a CPE into equivalent circuits enables excellent fitting to impedance data over wide frequency and temperature ranges.

In carrying out equivalent circuit analysis of impedance data, there are two stages to the analysis. First, is to find an equivalent circuit that accurately fits the data with the objective, ideally, of identifying a unique equivalent circuit rather than a number of equally plausible equivalent circuits. Second, is to find a physical interpretation of the parameters in the equivalent circuit.

The first stage requires the testing of various R and C circuit combinations in order to obtain a realistic fit to experimental data; to assist in the search, a valuable guide to the most likely equivalent circuit comes from inspection of impedance data in various formalisms based on the complex functions: impedance, Z^*, modulus, M^*, admittance, Y^*, and permittivity, ε^* (Refs. [10–12]). A given data set can be represented in any of these formalisms, as either complex plane plots or spectroscopic plots of their real and imaginary components; the dielectrics community also makes use of tan δ plots, which correspond to the ratio of imaginary to real components of the permittivity. The different impedance formalisms have different in-built weighting factors toward the data and it is necessary, therefore, to test the fit of a proposed equivalent circuit in each of the formalisms.

It is clear from the attempts at circuit analysis using various R,C combinations that, at certain frequencies and temperatures, single-valued R and C parameters can be identified. However, it is not possible to model the very extensive frequency dispersions that are seen in for instance, Y' and C' spectroscopic plots unless a distribution of relaxation times associated with the R,C components is considered. For this reason, the next stage in seeking an appropriate equivalent circuit is to consider introduction of a CPE into the equivalent circuit; as shown here, excellent fits to the experimental data are then obtained. At low temperatures, below ~ 700 K, a master circuit, Fig. 7(a), is used, which fits the data at the lowest temperatures ≤ 60 K; with increasing

temperature the master circuit simplifies, first by elimination of resistance R_1 and subsequently, by elimination of the CPE and capacitance C_1.

At the highest temperatures ≥ 873 K, modification of the equivalent circuit is necessary since the sample shows a small amount of residual leakage conduction. This is represented by a circuit element consisting of a resistor-capacitor-CPE in parallel. We do not give these high temperature data any further consideration, however, since they have no bearing on the low temperature relaxor phenomena.

Given that we now have a master equivalent circuit, Fig. 7(a), and its simplified versions, Figs. 7(b) and 7(c), that fits the low temperature experimental data, it is appropriate to consider the significance of the various circuit elements. The simplest data sets occur above 120 K for which the data can be represented by a single, frequency-independent capacitor and therefore, the sample behaves as an ideal dielectric with no measurable conductivity. In this range, the value of the sample bulk permittivity, calculated from the C_2 data, Table I, decreases from ~ 290 at 120 K to ~ 230 at 320 K.

At lower temperatures, below ~ 120 K, polar regions in the crystal structure, associated either with A-sites containing Bi and Zn or B-sites containing Nb and Ti, start to generate a significant, but small displacive or polarization component that can respond to the *ac* measuring field. It is found that addition of a series CPE to the equivalent circuit is necessary to model the electrical properties. This means that the displacive/polarization phenomena are frequency- and therefore time-dependent and more specifically, that cooperative interactions between the individual polar units are involved. The polar displacements and polarization in this region are easiest at 120 K, at which temperature the value of capacitance C_1 increases to a maximum. Above 120 K, capacitance C_1 is not an identifiable parameter in the equivalent circuit and the material behaves as a simple capacitor. We therefore identify 120 K as the Burns temperature. It is not clear whether the polar displacements no longer exist above 120 K or whether they are undetected in the impedance analysis since $C_1 \gg C_2$.

With decreasing temperature below 120 K, the polarization process becomes more sluggish and the value of C_1 decreases. With further reduction in temperature, an additional circuit element R_1 is required to fit the data and it appears that the condition is reached at which the polar fluctuations coalesce to form nanodomains: the parameter R_1 may represent the difficulty of the cooperative displacements associated with nanodomain reorientation. From the temperature dependence of R_1, detectable domain formation appears below $\sim 65(5)$ K; at lower temperatures, R_1 increases as the domains become increasingly frozen and more difficult to reorient. This interpretation is consistent with the idea of domain freezing at the Vogel-Tamman temperature T_{vf}, 10 K (Refs. [13–16]) although our analysis does not lead to characterization of a specific freezing temperature.

The analysis presented here is, therefore, partially consistent with the conventional approach to relaxor ferroelectrics. The Burns temperature[16,17] can be recognized, above which the material behaves as a simple capacitor. The Vogel-Tamman condition can be identified below which the

polar domains are essentially frozen, although from the temperature-dependence of R_1, it is not possible to assign this to a specific temperature. In addition, however, identification of the parameters R_1 associated with domain reorientation, C_1 associated with polar displacements of individual dipoles and CPE_1 which represents the frequency-dependent cooperative interaction between dipole displacements, provide additional quantifiable parameters to describe the relaxor phenomenon.

It is clear that BZNT is a perfect dielectric material at low temperature since there is no evidence of any leakage conductivity which would be represented by a finite resistance in parallel with the remainder of the equivalent circuit, i.e., element C_2 in Fig. 7 is a perfect blocking capacitor. An equivalent circuit that is often used to represent dielectric relaxation processes within an insulating system is shown in Fig. 7(d). This is a circuit composed of ideal, frequency-independent circuit elements; the master circuit, Fig. 7(a), that is deduced here and used to model relaxor data may be regarded as an extension of the ideal dielectric relaxation circuit (d) in which introduction of the CPE adds frequency-dependent elements to the single-valued components R_1 and C_1.

A. Physical origin of the constant phase element

A CPE may be regarded as a combination of a frequency-dependent resistance, $A\omega^n$ in parallel with a frequency-dependent capacitance $B\omega^n$. A and B are interrelated (Eq. 3) and the relative importance of the two components is given by the magnitude of the power law, n, parameter. Thus, if $n = 0$, the CPE reduces to a simple resistance of magnitude A whereas if $n = 1$, the CPE reduces to a simple capacitor of magnitude B. For intermediate values of n, the magnitudes of both components are frequency-dependent. In circuit Fig. 7(a), the circuit element used to model data consists of the CPE in parallel with both a resistance and a capacitance. This means that both the resistive and capacitive components of the circuit contain both frequency- independent and frequency-dependent components.

In the literature, there appears to be no clear view as to the physical origin of CPEs and they are often regarded mainly as circuit fitting parameters. In the present case, we are able to offer some suggestions, as follows. The CPE represents time-dependent phenomena which, in the case of polarization fluctuations in a relaxor, may be an indicator of the cooperative nature of the fluctuations of individual dipoles. Specifically, fluctuating dipoles interact with their surroundings. At temperatures above the Burns temperature, where the data can be represented as a simple capacitor, any polarization fluctuations are small, occur independently of the surroundings and do not involve a CPE over the timescales of the impedance measurements; at temperatures between 60 and 120 K polarization fluctuations occur, are cooperative and require the inclusion of the CPE; at the lowest temperatures, < 60 K, the CPE is still necessary, but at these temperatures polar nanodomains coalesce and an additional resistive term is required to model the overall domain reorientation.

V. CONCLUSIONS

Using equivalent circuit analysis, the dielectric properties of BZNT relaxor have been satisfactorily modeled. A master circuit is derived that is based on a standard circuit for dielectric relaxation processes consisting of a parallel RC element in series with a blocking capacitor to which is added a parallel CPE that effectively converts the R and C components of the parallel RC element into a frequency-dependent resistor and capacitor. The use of equivalent circuit analysis has several beneficial features in comparison with the usual methods of data presentation involving fixed-frequency temperature sweeps of permittivity and tan δ.

First, the data can be accurately modeled by an equivalent circuit, which is fully tested by showing that, within errors, the data fit the proposed circuit in a range of electrical formalisms and presentation methods; this is important since different formalisms have different in-built weighting factors as a function of frequency.

Second, it shows the key role of the CPE and thereby, the frequency-dependent resistor and capacitor, in accounting for the frequency-dependent electrical properties of the relaxor.

Third, it allows extraction of a resistance parameter, R_1, which is a direct measure of the difficulties of domain reorientation and quantifies how this difficulty increases with decreasing temperature.

Fourth, it allows extraction of the value for the frequency independent component of the permittivity as a function of temperature and demonstrates that this capacitance is significantly higher than the overall measured capacitance of the sample. The measured capacitance is not a single-value parameter but represents a series combination of the R_1, C_1, CPE_1 and C_2 components; since capacitive components in series add as their reciprocals, the net effect of the blocking capacitance C_2 in the equivalent circuit is to reduce the overall measured capacitance of the sample.

[1]W. Ren, S. Trolier-McKinstry, C. A. Randall, and T. R. Shrout, J. Appl. Phys. **89**, 767 (2001).
[2]L. E. Cross, Ferroelectrics **151**, 305 (1994).
[3]J. C. Nino, M. T. Lanagan, and C. A. Randall, J. Mater. Res. **16**, 1460 (2001).
[4]S.-Y. Cho, H.-J. Youn, D.-W Kim, and K. S. Ban, J. Am. Ceram. Soc. **81**, 3038 (1998).
[5]S. L. Swartz and T. R. Shrout, U. S. patent 5,449, 652 (September 12 1995).
[6]K. Sudheendran and K. C. J. Raju, J. Am. Ceram. Soc. **92**, 1268 (2009).
[7]P. K. Davies and M. Valant, J. Mater. Sci. **34**, 5437 (1999).
[8]H. Wang, S. Kamba, H. Du, M. Zhang, C.-T. Chia, S. Veljko, S. Denisov, F. Kadlec, J. Petzelt and X. Yao, J. Appl. Phys. **100**, 014105 (2006).
[9]D. Huiling and X. Yi, Physica B **324**, 121 (2002).
[10]J. T. S. Irvine, D. C. Sinclair, and A. R. West, Adv. Mater. **2**, 132 (1990).
[11]D. P Almond and A. R. West, Solid State Ionics, **11**, 57 (1983).

[12]J. Ross MacDonald, *Impedance Spectroscopy: Emphasizing Solid Materials and Systems* (Wiley Interscience Publication, New York, 1987).

[13]S. Kumar and K. B. R. Varma, Adv. Sci. Lett. **3**, 20 (2010).

[14]S. Kamba, V. Porokhonskyy, A. Pashkin, V. Bovtun, J. C. Nino, S. T-. Mckinstry, C. A. Randall and M. Lanagan, Br. Ceram. Proc. **63**, 164 (2003).

[15]D. Viehland and W.-T. Huang, Ferroelectrics **158**, 301 (1994).

[16]V. Bovtun, J. Petzelt, V. Porokhonskyy, S. Kamba, T. Ostapchuk, M. Savinov, P. Samoukhina, P. Vilarinho and J. Baptista, Br. Ceram. Proc. **63**, 109 (2003).

[17]D. Viehland, Z. Xu, and D. A. Payne, J. Appl. Phys. **74**, 7454 (1993).